Measurement of the Stark shift of the $6s\,^2S_{1/2} \rightarrow 7p\,^2P_J$ transitions in atomic cesium

George Toh,[1] D. Antypas,[1,2] and D. S. Elliott[1,2]

[1]*School of Electrical and Computer Engineering, Purdue University, West Lafayette, Indiana 47907, USA*

[2]*Department of Physics and Astronomy, Purdue University, West Lafayette, Indiana 47907, USA*

(Received 3 March 2014; revised manuscript received 4 April 2014; published 24 April 2014)

We report measurements of the Stark shift of the cesium $6s\,^2S_{1/2} \rightarrow 7p\,^2P_{3/2}$ and $6s\,^2S_{1/2} \rightarrow 7p\,^2P_{1/2}$ transitions at $\lambda = 456$ and 459 nm, respectively, in an atomic beam. From these, we determine the static scalar polarizability for both $7P$ states and the tensor polarizability for the $7P_{3/2}$ state. The fractional uncertainty of the scalar polarizabilities is ∼0.18%, while that of the tensor term is 0.66%. These measurements allow a precise determination of the reduced radial matrix elements $\langle 7P_{1/2}||r||6D_{3/2}\rangle = 17.92\,(3)\,a_0$ and $\langle 7P_{3/2}||r||6D_{5/2}\rangle = 24.28\,(6)\,a_0$, providing a sensitive test and critical confirmation of theoretical models of the Cs atom, which has played a central role in parity nonconservation measurements.

DOI: 10.1103/PhysRevA.89.042512 PACS number(s): 32.10.Dk, 32.60.+i

I. INTRODUCTION

The high precision attainable in measurements of the Stark shift of atomic transition frequencies makes them sensitive tests of theoretically determined radial matrix elements. Atomic cesium, which has played a central role in parity nonconservation measurements over the past 40 years [1–6], is of particular interest in this regard, where accurate determinations of electric dipole matrix elements, experimental [7–15] and theoretical [16–18], are critical for precise determination of the weak charge. In this report, we discuss our recent measurements of the scalar static polarizabilities α_0 of the $7p\,^2P_{1/2}$ and $7p\,^2P_{3/2}$ states of atomic cesium and the tensor static polarizability α_2 of the $7p\,^2P_{3/2}$ state. We use our measurements to derive the reduced radial matrix elements $\langle 7P_{1/2}||r||6D_{3/2}\rangle$ and $\langle 7P_{3/2}||r||6D_{5/2}\rangle$, with fractional uncertainties of 0.17 and 0.25%, respectively.

The tensor polarizability for the $7p\,^2P_{3/2}$ state in cesium has been measured previously using the level-crossing technique by Khadjavi, Lurio, and Happer [19] and by Khvostenko and Chaika [20], with a measurement uncertainty of a few percent in each case. A subsequent measurement of this tensor polarizability, as well as the scalar polarizability α_0 for both $7p\,^2P_J$ lines, was reported by Domelunksen [21], with a comparable uncertainty. In the present work, we are able to improve the precision of each of these polarizabilities. To achieve this, we use narrow-band, frequency-stabilized diode lasers to excite the $6s\,^2S_{1/2} \rightarrow 7p\,^2P_J$ transitions in a nearly Doppler-free atomic beam geometry, allowing us to spectrally resolve the various hyperfine components of the transitions (shown schematically in Fig. 1). We report values of α_0 with an uncertainty of ∼0.18% and of α_2 with an uncertainty of 0.66%. Our results are in good agreement with early theoretical values based upon Coulomb potentials [23], as well as the more recent results of Iskrenova-Tchoukova, Safronova, and Safronova [17], who use a relativistic all-order method to calculate transition moments and a sum-over-states method to determine the polarizabilities.

Upon application of a dc electric field of magnitude E_0 to an atomic system, the energy of a bound state of that atom is shifted through the quadratic Stark effect by the amount

$$\Delta E = -\tfrac{1}{2}\alpha E_0^2, \tag{1}$$

where α is the polarizability of the atomic level. For a level of electronic angular momentum J, the polarizability α can be expressed in terms of its scalar (α_0) and tensor (α_2) components as

$$\alpha = \alpha_0 + \alpha_2 \frac{3m_J^2 - J(J+1)}{J(2J-1)}, \tag{2}$$

where m_J is the projection of the angular momentum on the z axis. The scalar term represents an overall shift of all components of the level together, while α_2 describes a splitting of the state into its various magnetic components. For $J = 0$ or $\frac{1}{2}$, the α_2 term in Eq. (2) vanishes, and the level is shifted in energy but remains unsplit. For levels that exhibit hyperfine structure and have angular momentum $J \geqslant 1$, the Stark effect produces a much richer spectrum. Schmieder [24] showed that the polarizability α of the (F, m_F) hyperfine component is of the form

$$\alpha = \alpha_0 + \alpha_2\, Q_{F,\tilde{F};|m_F|}, \tag{3}$$

where the matrix $Q_{F,\tilde{F};|m_F|}$ describes the mixing of states of unequal F (F and $\tilde{F}$ in this expression), but equal m_F, by the static field. (We use the usual notation here, with F representing the total atomic angular momentum, including nuclear spin I, and m_F representing the projection of F on the z axis.) The scalar part of the polarizability shifts all hyperfine and magnetic sublevels equally, while the tensor part causes the spectrum to diverge into a series of individual lines. As an illustration, we show an uncalibrated, partial Stark spectrum of the $6s\,^2S_{1/2} \rightarrow 7p\,^2P_{3/2}$ transition at $E_0 =$ 12 kV/cm in Fig. 2(a). We label each peak with F' and m'_F of the $7p\,^2P_{3/2}$ state. In contrast, each hyperfine line of the $6s\,^2S_{1/2} \rightarrow 7p\,^2P_{1/2}$, while shifted by the Stark effect, remains a single line. In the following, we will discuss our experimental observations of the Stark spectrum of the two transitions $6s\,^2S_{1/2} \rightarrow 7p\,^2P_J$, $J = \frac{1}{2}$ and $\frac{3}{2}$, in atomic cesium, and from these our determination of the scalar and tensor polarizabilities.

II. DESCRIPTION OF APPARATUS

The general principle of the measurement is similar to that of several other recent works [25–28]. We use the output of a single, narrow-band tunable laser source, which we split into

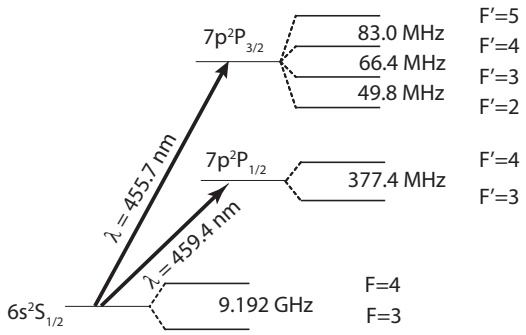

FIG. 1. Energy-level diagram of atomic cesium, showing the levels relevant to these measurements. Hyperfine splittings of the $7P$ states are taken from Ref. [22].

two separate beams, labeled the reference and Stark beams in Fig. 3. Using an electro-optic modulator (EOM) and an acousto-optic modulator (AOM) to offset the frequencies of these two beams, we concurrently bring the reference beam into resonance with the cesium transition in a field-free vapor cell (the reference cell) and the Stark beam into resonance with the transition in cesium atoms to which a uniform electric field has been applied. The difference between the frequency offsets of these two beams, which depend only on the rf frequencies driving the modulators, equals the Stark shift of the resonance. This eliminates the requirement for calibration of the laser frequency scan, which can be problematic at the precision required in these measurements. The Doppler broadening of the resonances is largely suppressed in our measurements, allowing us to resolve the hyperfine structure of the transitions

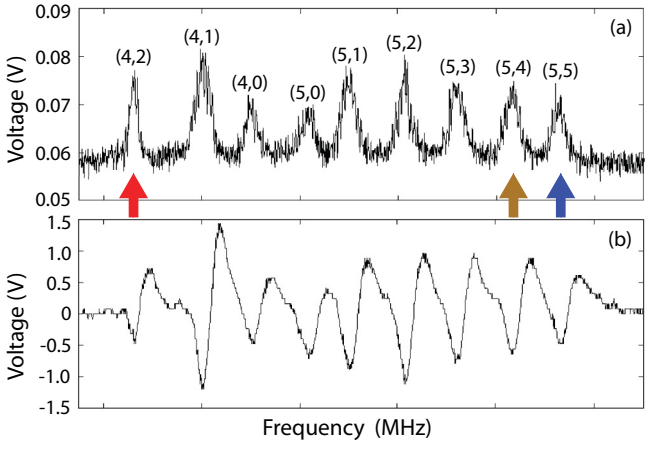

FIG. 2. (Color online) (a) An uncalibrated partial Stark spectrum of the $6s\,^2S_{1/2}, F = 4 \rightarrow 7p\,^2P_{3/2}$ transition at $E_0 = 6$ kV/cm showing the splitting of the lines. The notation above each peak indicates $(F', |m'_F|)$ of the $7p\,^2P_{3/2}$ state. The arrows indicate the peaks used in our measurements, and the frequency difference between the red and blue arrows is approximately 155 MHz. (b) The derivative signal of the same spectrum. There is a small mismatch between the error signal zero crossing and the center of the signal peaks due to the long integration time constant on our lock-in amplifier. This does not affect our results because we fix the EOM frequency when making a measurement.

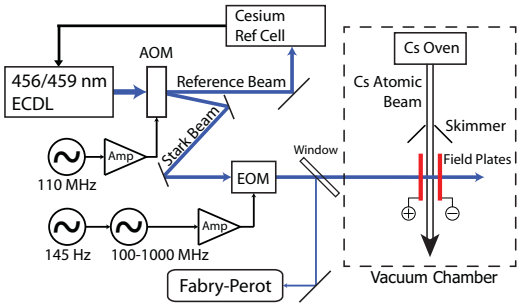

FIG. 3. (Color online) Diagram of the experimental configuration. The external cavity diode laser (ECDL) generates light at 455.7 or 459.4 nm, resonant with the $6s\,^2S_{1/2} \rightarrow 7p\,^2P_{3/2}$ or $6s\,^2S_{1/2} \rightarrow 7p\,^2P_{1/2}$ transition, respectively. The frequency of this beam is shifted in the acousto-optic modulator (AOM), and sidebands imposed in the electro-optic modulator (EOM), before crossing the atomic beam inside the vacuum chamber at a perpendicular crossing angle. We monitor the sideband structure of the Stark beam with the Fabry-Perot interferometer.

and also allowing us to use relatively low dc electric-field strengths in our measurements.

The laser for these measurements, which we operate at wavelengths of 455.7 (for the $6s\,^2S_{1/2} \rightarrow 7p\,^2P_{3/2}$ transition) or 459.4 nm (for the $6s\,^2S_{1/2} \rightarrow 7p\,^2P_{1/2}$ transition), is a home-made external cavity diode laser (ECDL) using an antireflection coated laser diode, which generates approximately 10 mW of optical power. We diffract the output beam in an AOM and use the first-order diffracted beam, whose frequency is $f_l + f_{\mathrm{AO}}$ (where f_l is the frequency of the laser output and $f_{\mathrm{AO}} = 110.0$ MHz is the AOM drive frequency), for the experiment (i.e., this is the Stark beam). The 110-MHz drive signal is produced by a synthesized signal generator and amplified by an rf amplifier. We direct the undiffracted beam, which we use as our reference beam, into a field-free cesium vapor cell and frequency lock the laser to one hyperfine component of the Doppler-free saturated absorption spectrum (the $6s\,^2S_{1/2}, F = 4 \rightarrow 7p\,^2P_{1/2}, F = 4$ line at $\lambda = 459$ nm or the $6s\,^2S_{1/2}, F = 4 \rightarrow 7p\,^2P_{3/2}, F = 5$ line at $\lambda = 456$ nm) of this spectrum. To obtain an error signal for locking to the peak of the hyperfine line, we dither the laser injection current at 30 kHz. In either case, the laser frequency f_l is resonant with and stabilized to the unshifted atomic resonance, f_a. The linewidth of the laser spectrum is <1 MHz. Because the absorption strengths of these transitions are relatively weak, we have to heat the cesium vapor cell to a temperature in the range 80–110 °C to obtain sufficient Cs density within the cell.

We impose optical sidebands on the spectrum of the Stark beam by modulating its phase in a traveling-wave EOM, driven by a separate signal generator and amplifier at a frequency f_{EO}, where we can adjust f_{EO} to any frequency in the range from 110 to 1000 MHz. We use the lower-frequency sideband, whose frequency is $f_l + f_{\mathrm{AO}} - f_{\mathrm{EO}}$, to excite the Stark-shifted absorption resonance in the atomic beam. We control the frequency difference between the reference beam and the Stark beam in order to make our measurements (see the following sections).

The cesium atom beam is formed inside an aluminum vacuum chamber pumped with a turbomolecular pump to a pressure of 5×10^{-6} torr. We use an effusive cesium oven with a nozzle consisting of an array of stainless steel hypodermic needle tubes to form the atom beam. More details are available in our earlier publications [29,30]. This oven and nozzle generate a beam of dimension 12×8 mm near the nozzle. We insert an atomic beam aperture (labeled skimmer in Fig. 3) before the interaction region to further reduce the width of the atomic beam to $\sim 1/2$ the spacing of the field plates. This reduces the accumulation of cesium on the electric-field plates. The spectral width of the $6s \rightarrow 7p$ absorption lines in our beam geometry is $\sim$6 MHz full width at half maximum, largely due to Doppler broadening in the slightly diverging atomic beam. The natural linewidths of these transitions, corresponding to the 133-ns lifetime of $7P_{3/2}$ and the 155-ns lifetime of the $7P_{1/2}$ state [31–33], are 1.2 and 1.0 MHz, respectively.

The uniformity of the static electric field and the precision with which this field can be determined depend critically on the parallel conducting field plates used to generate this field. We construct these field plates from a pair of 76.2 × 25.4-mm (3 × 1-in.) microscope glass slides, coated on the inside surfaces with a thin conducting layer of indium tin oxide. These field plates are spaced by 4.928(4) mm [0.194 00(15) in.] and are mounted inside an aluminum framework with external ceramic posts using a vacuum compatible epoxy. (The number enclosed within parentheses following these parameters indicates our estimate of the uncertainty.) We evaluated the nonuniformity of the electric field within the interaction region due to fringing effects using a commercial software package and found that this variation is less than a part in 10^5.

During assembly, we spaced the field plates with a set of carefully selected ceramic spacers to assure a high degree of parallelism, then removed the spacers after the epoxy had dried. (We observed drifts in some of our early Stark-shift measurements, which we attributed to an accumulation of cesium on the internal spacers used for those measurements. These drifts were absent after we removed the internal spacers.) We estimate the 0.000 15-in. uncertainty in the spacing of the glass slides based on the relative ease with which we can slip calibrated ceramic beads, whose lengths we measured to ±0.000 05 in., at various locations near the central region of the field plates, similar to the technique described in Refs. [26,27]. We also measured the parallelism of the plates by reflecting a HeNe laser beam from the two surfaces and observing the spacing of the fringes formed by the interference of the two reflected beams. We estimate that the angle between the two plates was less than 0.15 mrad. This high degree of parallelism between the field plates is consistent with our estimate of the variation of the plate spacing over the width of the plates.

We use a pair of stable high-voltage sources to bias the field plates, one plate positively biased and the other negative. Between sets of data, we switch the polarity of the field plates. We measure the voltage applied to each field plate using an Ohmcraft 1000:1 high-voltage resistive divider, which we have carefully checked and calibrated for nonlinearity and stability. The fractional uncertainty in the voltage measurement of each field plate is $\sim 2 \times 10^{-5}$.

Consistent with the treatment by Schmieder [24], we define the z axis of the atomic system as the direction of the applied field E_0. While the Stark beam for these measurements propagates in a direction $\hat{\mathbf{k}}$ nearly parallel to this z axis, and its polarization state is linear, the experiment is relatively insensitive to either of these conditions, since the ground-state components are degenerate, and the various peaks in the Stark spectrum correspond to different hyperfine components of the excited state alone. Changes in polarization or imperfect alignment of $\hat{\mathbf{k}}$ with the z axis only change the relative height of the peaks in the Stark spectrum, but not their frequency. By contrast, it is important that the laser beam propagates in a direction perpendicular to the atomic velocity to assure narrow absorption linewidths and to minimize the Doppler shift of the lines. Using an alignment laser, we mount the parallel field plates inside the vacuum system centered on and parallel to the atomic beam. In addition, we observe the reflection of the Stark beam from the field plates and adjust this beam to normal incidence on the field plates. After these alignment steps, only a minor adjustment of the Stark beam direction $\hat{\mathbf{k}}$ is necessary to minimize the Doppler shift of the resonance in the atomic beam, which we determine by zeroing the applied field and comparing the absorption resonance in the atomic beam to that of the reference cell.

In order to detect the absorption resonances in the atomic beam, we use the detection system that we developed earlier [29,30] for sensitive measurement of highly forbidden optical transitions. We based this system on a technique reported earlier in Ref. [2]. The population of the cesium atoms as they effuse from the oven is equally distributed among each of the $F = 3$ and 4 hyperfine components of the ground state. Before the atoms interact with the blue laser, we transfer all of the atoms into the $F = 4$ level by optically pumping the population with the output of an 852-nm ECDL tuned to the $6s\,^2S_{1/2}$, $F = 3 \rightarrow 6p\,^2P_{3/2}$, $F' = 4$ hyperfine transition of the D_2 resonance line. After interacting with the blue laser, the population in the initially empty $F = 3$ ground state is a measure of the excitation rate by the Stark beam to the $7P$ state, since these atoms decay spontaneously back to the ground state. We detect this population using the output of a second ECDL tuned to the D_2 line at 852 nm (in this case resonant with the $6s\,^2S_{1/2}$, $F = 3 \rightarrow 6p\,^2P_{3/2}$, $F' = 2$ cycling transition) and a large area photodiode to measure the scattered optical power in this region.

We use a lock-in amplifier for phase-sensitive detection of the photodiode current in order to improve the sensitivity of the measurement. We dither the frequency of the EO sideband at 145 Hz (with a 1-MHz amplitude), which modulates the rate of absorption by the atoms. The derivative signal produced by the lock-in amplifier, illustrated in Fig. 2(b), is a dispersion shaped resonance of width $\sim$6 MHz. The zero crossing is well suited for determination of the line center.

During the course of our measurements, we found that the amplitude of the optical sideband of the Stark beam, as monitored with a scanning Fabry-Perot interferometer, varied across the 100–1000-MHz spectrum. To ensure that the optical power in the sideband used for the experiment is constant, we selected frequencies f_{EO} at which the sideband power is relatively uniform.

We must keep the laser intensity below the saturation intensity I_{sat} in order to minimize power broadening and light shifts. The laser intensity for these measurements is 4 mW/cm^2, of which only $\sim$1/3 is in the lower sideband that interacts with the atoms. Using the reduced matrix dipole matrix elements for these transitions [15], we estimate that the saturation intensity I_{sat} of the $6s\ ^2S_{1/2} \rightarrow 7p\ ^2P_{3/2}$ transition is about 15 mW/cm^2, while that of the $6s\ ^2S_{1/2} \rightarrow 7p\ ^2P_{1/2}$ line is about 50 mW/cm^2. Therefore, the sideband intensity is well below I_{sat} in both cases.

A. Scalar polarizability of $7p\ ^2P_{1/2}$

For our determination of the polarizability α_0 of the $7p\ ^2P_{1/2}$ state, we first set the EO modulation frequency f_{EO} to one of seven predetermined values in the range between 110 and 1000 MHz. (The minimum of this range is the AO drive frequency, and corresponds to a zero Stark shift, while the maximum frequency is the maximum frequency of our signal generator.) At each value of f_{EO}, we adjust the voltage applied to the plates to shift the transition into resonance with the lower sideband of the Stark beam. In Fig. 4, we show one set of these data, plotted as f_{EO} vs E_0^2. The solid line indicates the result of a linear least-squares fit with two adjustable parameters, the intercept and the slope.

The intercept of this fitted line is 109.8 (2) MHz, consistent with the 110.0-MHz frequency offset imposed by the AOM. The slope of this line is 3.6417 (12) MHz/(kV/cm)^2 and is equal to half the difference between the polarizabilities of the $7P_{1/2}$ state and the $6S_{1/2}$ state, $\frac{1}{2}\{\alpha_0(7P_{1/2}) - \alpha_0(6S_{1/2})\}$. The uncertainty of 0.0012 MHz/(kV/cm)^2 is statistical and is determined from the scatter of the data points from the linear fit to the data. We show the difference between the data points

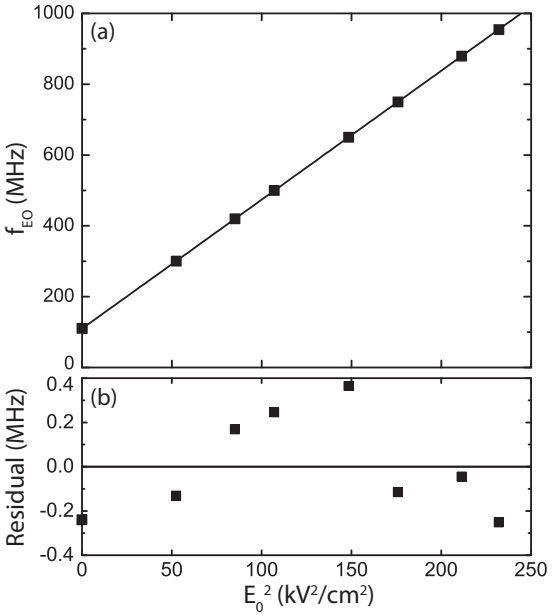

FIG. 4. (a) A plot of f_{EO} vs E_0^2 for the $6s\ ^2S_{1/2} \rightarrow 7p\ ^2P_{1/2}$ transition. Experimental data are shown by the square points, while the solid line shows the result of a linear least-squares fit. The residual error of each data point is shown in (b).

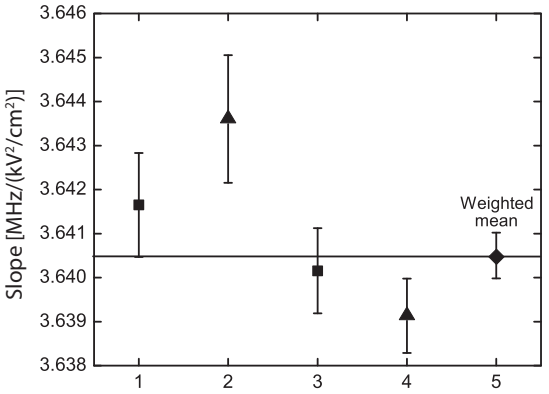

FIG. 5. Summary of the four measurements of $\frac{1}{2}\{\alpha_0(7P_{1/2}) - \alpha_0(6S_{1/2})\}$. Error bars shown are statistical only. Square data points were obtained with the electric field in the same direction as the Stark beam. For the triangular data points, the measurements were made with the electric-field orientation reversed. The fifth point (diamond shaped) and horizontal line denote the weighted average.

and the linear fit, in Fig. 4(b). The rms residual for this set of data is 0.22 MHz.

We measured the Stark shift of the $7P_{1/2}$ state four times, reversing the direction of the electric field between sets of data, and observed no variation correlated to electric-field orientation. We show the slope $\frac{1}{2}\{\alpha_0(7P_{1/2}) - \alpha_0(6S_{1/2})\}$ resulting from each of these measurements in Fig. 5. The error bars shown in the figure indicate the statistical uncertainty for each data point. The weighted average of the four measurements yields $\frac{1}{2}\{\alpha_0(7P_{1/2}) - \alpha_0(6S_{1/2})\} = 3.6405\ (6)$ MHz/(kV/cm)^2, as indicated by the diamond-shaped data point and horizontal line in Fig. 5. The reduced χ^2 for these measurements is 4.14, indicating that the measurement uncertainty is larger than the statistical uncertainty. We have not scaled the statistical error despite the large χ^2 factor. As we will discuss in Sec. III, the overall measurement uncertainty is dominated by the uncertainty in the field plate spacing, and scaling the statistical error has little impact on our final result. Using the ground-state polarizability $\alpha_0(6S_{1/2}) = 0.099\,78\ (15)$ MHz/(kV/cm)^2 from Ref. [12], we find $\alpha_0 = 7.3808\ (12)$ MHz/(kV/cm)^2, where the number in parentheses denotes the statistical error only. In atomic units, this is equivalent to 29 662 (5) a_0^3.

B. Scalar and tensor polarizability of $7p\ ^2P_{3/2}$

We base our determinations of α_0 and α_2 for the $7p\ ^2P_{3/2}$ line on two lines in the Stark-shifted spectrum, namely, the $(F', |m'_F|) = (5,5)$ line and the (4,2) line. We chose these particular m_F peaks because they are well resolved from other peaks in the spectrum, as shown in Fig. 2, and because their frequency difference due to the Stark shift is large, allowing for a more precise evaluation of α_2. From Eq. (3), the polarizability of the $F' = 5$, $m_F = \pm 5$ components is $\alpha_0 + \alpha_2$. Our process for determination of the sum $\alpha_0 + \alpha_2$ for the $7p\ ^2P_{3/2}$ state then is similar to that of α_0 for the $7p\ ^2P_{1/2}$, described in the last section. With the reference laser frequency f_l tuned and locked to the $6s\ ^2S_{1/2}$, $F = 4 \rightarrow 7p\ ^2P_{3/2}$, $F' = 5$ resonance in the reference cell, we adjust the frequency f_{EO} of the signal

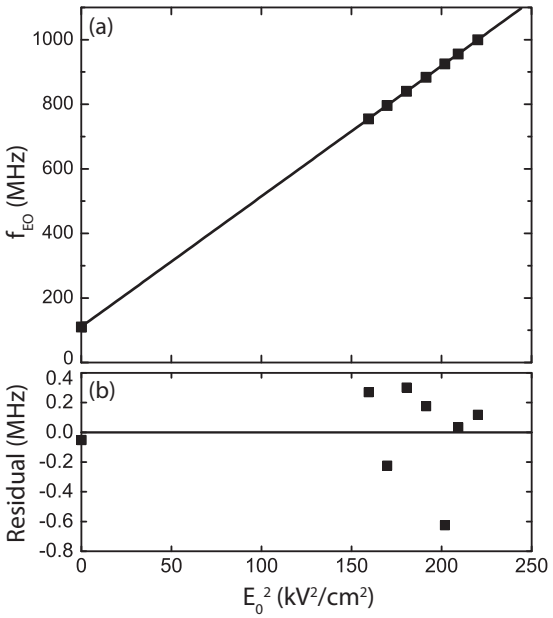

FIG. 6. (a) An example of one data set of f_{EO} vs E_0^2 for $6s\,^2S_{1/2}$, $F = 4$, $m_F = \pm 4 \rightarrow 7p\,^2P_{3/2}$, $F' = 5$, $m'_F = \pm 5$. The straight line is the result of a linear least-squares fit to the data points. (b) The residual between the data points and the straight line.

applied to the EOM to one of seven values in the range from 700 to 1000 MHz. (Below 700 MHz, the various peaks within the Stark spectrum partially overlap, introducing errors in the measurements of the line center.) Then we vary the voltage applied to the field plates to bring the (5,5) peak into resonance. We also take one measurement at zero electric field, varying f_{EO} to find the line center.

We show an example of one data set in Fig. 6. The result of a linear least-squares fit, represented by the straight line in this figure, yields an intercept of 110.7 (3) MHz and a slope of $\frac{1}{2}\{\alpha_0(7P_{3/2}) + \alpha_2(7P_{3/2}) - \alpha_0(6S_{1/2})\} = 4.0386\,(18)$ MHz/(kV/cm)^2. We show the deviation of each of the data points from the fitted line in Fig. 6(b). The rms residual is 0.3 MHz. We repeat this measurement with the electric-field orientation reversed and obtain a result which is in good agreement with our first measurement. Using the two measurements, we determine a weighted average slope of $\frac{1}{2}\{\alpha_0(7P_{3/2}) + \alpha_2(7P_{3/2}) - \alpha_0(6S_{1/2})\} = 4.0389\,(13)$ MHz/(kV/cm)^2. Using $\alpha_0(6S_{1/2})$ from Ref. [12], we obtain $\alpha_0 + \alpha_2 = 8.1776\ (26)$ MHz/(kV/cm)^2 for the $7p\,^2P_{3/2}$ state. This uncertainty accounts for statistical effects only.

As we discussed earlier, the frequency difference between the hyperfine components of the Stark spectrum is quantified through the tensor polarizability α_2, for which we base our determination on a measurement of the frequency difference between the (5,5) peak and the (4,2) peak. At zero field, the frequency difference between these peaks is the hyperfine splitting $f_{4-5} = 83.025(30)$ MHz of the $7p\,^2P_{3/2}$ state [22]. We measure this frequency difference by fixing the electric field E_0 and adjusting the frequency f_{EO} to bring the Stark laser sideband into resonance with each sublevel. For each of three voltage levels, we repeat the measurement with the field direction reversed. In order to determine the value of α_2, we fit the diagonalized matrix Q to the data points. In this case, we fixed the value of $\alpha_0 + \alpha_2$ to the value 8.1776 (26) MHz/(kV/cm)^2, as discussed above, and used Eqs. (40a) and (41) from Ref. [24] to generate curves for varying values of α_2. The least rms deviation between the calculated and measured frequency difference between the $(F', |m'_F|) = (5,5)$ and (4,2) Stark-shifted frequencies yields $\alpha_2 = -1.0981\ (65)$ MHz/(kV/cm)$^2 = -4413\ (26)\ a_0^3$. In Fig. 7 we show the best-fit curves for the Stark-shifted hyperfine peaks vs E_0^2, with the scalar component of the Stark shift suppressed. The circles denote our experimental data points. We also show measurements of the $F' = 5$, $m'_F = 4$ sublevels in this figure. We did not use these values in the determination of α_2, since the smaller frequency difference between this peak and the (5, 5) peak gave these values a larger uncertainty. Combining our results for $\alpha_0 + \alpha_2$ and α_2 yields a value of $\alpha_0 = 9.2757\ (70)$ MHz/(kV/cm)^2, or 37 277 (28) a_0^3.

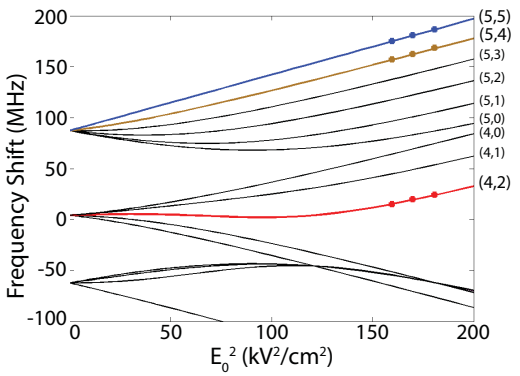

FIG. 7. (Color online) Frequency f_{EO} for the (5,5) (blue), (5,4) (gold), and (4,2) (red) peaks vs E_0^2 for determination of the tensor polarizability α_2. The solid lines are the calculated Stark shifts, less the α_0 terms, with α_2 adjusted to minimize the deviation with the data. The notation beside each line indicates $(F', |m'_F|)$ of the $7p\,^2P_{3/2}$ state.

III. MEASUREMENT ERRORS

The uncertainties in the polarizabilities that we presented in the previous section include only statistical effects derived from the scatter in the data points from the fitted lines. In addition, there are other experimental factors, as summarized in Table I, that we must consider. In this section, we

TABLE I. Sources of error, estimates of their uncertainties, and the resulting percentage uncertainty in α resulting from each source.

Source	Uncertainty	% of α
Field plate spacing	4 μm	0.16
Voltage divider ratio	0.005%	0.01
Voltage measurements	0.005%	0.01
Error signal line center	0.2 MHz	0.02
AOM drive frequency	10 kHz	0.01
EOM drive frequency	10 kHz	0.01
Beam alignment into chamber	0.05 mrad	0.01
Total systematic uncertainty		0.16

discuss these contributions and provide estimates of their magnitudes.

The largest uncertainty in our measurements is the systematic effect due to determination of the static electric-field strength. These uncertainties derive from the uncertainty in the field plate spacing (including the uncertainty in the measurement of this spacing d, as well as any nonuniformity in d), the uncertainty in the measurement of the voltage applied to the plates, and edge effects that reach into the center of the field plates. We have discussed the first of these in Sec. II, where we estimate an uncertainty of the plate spacing of 0.08%. Since the Stark shift depends on E_0^2, the corresponding uncertainty in the polarizabilities is twice as large, or 0.16%. We also described the voltage dividers that we used to measure the voltage applied to the field plates in Sec. II. This fractional uncertainty of 5×10^{-5} results in an uncertainty in the polarizabilities of 1×10^{-4}. We also list in Table I the measurement error of the volt meter as specified by the manufacturer.

We estimate that the precision with which we can measure the line center of each of the Stark-shifted line shapes is ± 0.2 MHz. This is primarily limited by signal asymmetry due to residual amplitude modulation of the Stark beam at 145 Hz. For instance, if the asymmetry of a dispersion-shaped resonance is 15% of the maximum error signal, as was typical of our measurements, the zero crossing is shifted by $\sim$0.2 MHz, assuming a 6-MHz linewidth of the absorption peak. Another limiting factor is dc offsets in the error signal, due to electronics and the overlap from adjacent peaks in the spectrum. We modeled the pulling of the line center due to adjacent peaks and found its effect on the polarizabilities to be less than 2×10^{-5}. We estimate that these limiting factors lead to a fractional uncertainty in the polarizabilities of 2×10^{-4}.

We also considered frequency shifts due to changes in the propagation direction of the laser beam. Such a change could introduce a Doppler shift in the line center of the resonance. Heating effects in the EOM could deflect the beam, for example. We have projected the Stark beam onto a screen 10 m beyond the EOM and were unable to observe any such deflection. We place an upper limit of 0.05 mrad on any such shift. Estimating the Doppler shift to be about 0.7 MHz/mrad, this shift corresponds to an uncertainty of less than 0.05 MHz. This limit is consistent with our observed rms residuals of the measured peak positions in Figs. 4 and 6 of 0.2 MHz.

In order to determine $\alpha_2(7P_{3/2})$ from our measurement of the frequency difference between the (5,5) and (4,2) peaks of the Stark spectrum, we used the hyperfine constants $a = 16.605(6)$ MHz and $b = -0.15(3)$ MHz from Ref. [22]. We consider here the effect of the uncertainty of these hyperfine constants on the uncertainties of the polarizabilities of the $7P_{3/2}$ state. By varying the values of the constants by one standard deviation and running the fitting function again, we can estimate their effect on our values of $\alpha_0(7P_{3/2})$ and $\alpha_2(7P_{3/2})$. This effect is estimated to be 0.21% for $\alpha_2(7P_{3/2})$ and $<0.02\%$ for $\alpha_0(7P_{3/2})$.

For our measurements of the scalar polarizabilities $\alpha_0(7P_{1/2})$ and $\alpha_0(7P_{3/2})$, only the 0.08% variability in the field plate spacing is significant. These effects contribute a 0.16% uncertainty. For the tensor polarizability $\alpha_2(7P_{3/2})$, there is an additional 0.21% error due to the uncertainty in the hyperfine constants. We add these uncertainties in quadrature with the statistical uncertainty stated earlier to obtain the total uncertainty. For the scalar polarizabilities $\alpha_0(7P_{1/2})$ and $\alpha_0(7P_{3/2})$, this results in an uncertainty in the final result of 0.17 and 0.18%, respectively. For the tensor polarizability $\alpha_2(7P_{3/2})$, the statistical uncertainty is the primary contributor to the 0.66% uncertainty in our result. In the next section, we present our final results for each and compare with prior experimental and theoretical determinations of these quantities.

IV. DISCUSSION

We present a summary of results for $\alpha_0(7P_{1/2})$, $\alpha_0(7P_{3/2})$, and $\alpha_2(7P_{3/2})$ in Table II, including the present results, as well as several past experimental and theoretical determinations. Each of our results is in good agreement with, but of higher precision than, past measurements reported in Refs. [19] and [21]. The measurement result for α_2 for the $7P_{3/2}$ in Ref. [20] differs by $\sim$10% from the others, including the present results. The theoretical calculations of van Wijngaarden and Li [23] and of Iskrenova-Tchoukova *et al.* [17] are in good agreement with our results for all three polarizabilities as well. The former does not report uncertainties. Our results differ from those of Ref. [17] by typically less than 1%, while their stated uncertainties are about 2%.

We can use our measurements of these scalar and tensor polarizabilities to determine the radial matrix elements $\langle 7P_{1/2}||r||6D_{3/2}\rangle$ and $\langle 7P_{3/2}||r||6D_{5/2}\rangle$. As presented in Ref. [17], the polarizability of the $7p\,^2P_{1/2}$ state is calculated from the sum over all dipole-coupled ns and nd states of the square of the radial matrix elements divided by the energy spacing. From Table III of Ref. [17], the primary contribution to this summation comes from the $6d\,^2D_{3/2}$ state, whose energy differs from that of the $7p\,^2P_{1/2}$ by only 823.471 cm^{-1} [34,35]. All other terms combined make up only 1150 (80) a_0^3 ($\sim$3.5% of the total). We use the theory values for each of these smaller contributions, which we subtract from our experimental value of 29 660 (50) a_0^3, to determine the contribution to $\alpha_0(7P_{1/2})$

TABLE II. Comparison of the polarizabilities determined in this work to those of prior experimental and theoretical works. All values are in units of $10^3\ a_0^3$.

	$7p\,^2P_{1/2}$	$7p\,^2P_{3/2}$	
Group	α_0	α_0	α_2
	Experiment		
Khadjavi *et al.* [19]			−4.33 (17)
Khvostenko and Chaika [20]			−3.9 (1)
Domelunksen [21]	29.5 (6)	37.8 (8)	−4.42 (12)
This work	29.66 (5)	37.28 (7)	−4.413 (29)
	Theory		
Van Wijngaarden and Li [23]	29.4	36.9	−4.28
Iskrenova-Tchoukova, *et al.* [17]	29.89 (70)	37.52 (75)	−4.41 (17)

due to the $6d\,^2D_{3/2}$ state alone. From this, we deduce a radial matrix element for this transition of 17.92 (3) a_0, with a relative uncertainty of 0.17%. This result compares very well with 17.99 a_0 from Table III of Ref. [17] and with 17.988 (48) a_0 presented in Ref. [28].

In a similar manner, we use our measurement of $\alpha_0(7P_{3/2}) = 37\,280\,(70)\,a_0^3$ to determine the radial matrix element $\langle 7P_{3/2}||r||6D_{5/2}\rangle$. In this case, the contribution to α_0 from this primary term is 85% of the total. We use the theory values for all the smaller contributions, as listed in Table IV of Ref. [17], which combine to 5846 (132) a_0^3. Subtracting this from our measured value for $\alpha_0(7P_{3/2})$ gives 31 430 (150) a_0^3 as the contribution to α_0 by the $6D_{3/2}$ state alone. With an energy difference of 685.29 cm^{-1} [34,35], the radial matrix element $\langle 7P_{3/2}||r||6D_{5/2}\rangle$ is 24.27 (6) a_0, in good agreement with the value of 24.35 a_0 from Table IV of Ref. [17]. This relative uncertainty is 0.25%. Finally, we use our measured value of α_2 to calculate $\langle 7P_{3/2}||r||6D_{5/2}\rangle$ by a second independent means and find 24.36 (18) a_0. The relative contribution of the other states to α_2 is relatively large and of opposite sign to that of the total. This result therefore depends heavily on theoretical values for the smaller terms. Still, the result is in agreement with the value determined through $\alpha_0(7P_{3/2})$, but of course of larger uncertainty. The weighted average of these two values is 24.28 (6) a_0.

V. CONCLUSION

We have described our experimental determinations of the Stark shift of the $6s\,^2S_{3/2} \rightarrow 7p\,^2P_J$ transitions for $J = \frac{1}{2}$ and $\frac{3}{2}$ in atomic cesium. Through use of a narrowband, frequency-stabilized diode laser and Doppler-free techniques, the precision of our measurements is higher than that of previous measurements. We derive the static scalar polarizabilities of the $7p\,^2P_{1/2}$ and $7p\,^2P_{3/2}$ states, as well as the tensor polarizability of the $7p\,^2P_{3/2}$ state. These polarizabilities allow a precise determination of the radial matrix elements $\langle 7P_{1/2}||r||6D_{3/2}\rangle$ and $\langle 7P_{3/2}||r||6D_{5/2}\rangle$. The precision of these matrix elements, and their excellent agreement with theoretical results of Refs. [17] and [28], provide strong confirmation of the atomic model used in those calculations.

ACKNOWLEDGMENT

This material is based upon work supported by the NSF under Grant No. PHY-0970041.

[1] M. A. Bouchiat and C. Bouchiat, J. Phys. **36**, 493 (1975).
[2] C. S. Wood, S. C. Bennett, D. Cho, B. P. Masterson, J. L. Roberts, C. E. Tanner, and C. E. Wieman, Science **275**, 1759 (1997).
[3] W. R. Johnson, M. S. Safronova, and U. I. Safronova, Phys. Rev. A **67**, 062106 (2003).
[4] M. Lintz, J. Guéna, and M.-A. Bouchiat, Eur. Phys. J. A **32**, 525 (2007).
[5] S. G. Porsev, K. Beloy, and A. Derevianko, Phys. Rev. Lett. **102**, 181601 (2009).
[6] B. M. Roberts, V. A. Dzuba, and V. V. Flambaum, Phys. Rev. A **87**, 054502 (2013).
[7] L. Young, W. T. Hill, S. J. Sibener, S. D. Price, C. E. Tanner, C. E. Wieman, and S. R. Leone, Phys. Rev. A **50**, 2174 (1994).
[8] R. J. Rafac and C. E. Tanner, Phys. Rev. A **58**, 1087 (1998).
[9] R. J. Rafac, C. E. Tanner, A. E. Livingston, and H. G. Berry, Phys. Rev. A **60**, 3648 (1999).
[10] A. Derevianko and S. G. Porsev, Phys. Rev. A **65**, 053403 (2002).
[11] A. A. Vasilyev, I. M. Savukov, M. S. Safronova, and H. G. Berry, Phys. Rev. A **66**, 020101 (2002).
[12] J. M. Amini and H. Gould, Phys. Rev. Lett. **91**, 153001 (2003).
[13] A. Sieradzan, M. D. Havey, and M. S. Safronova, Phys. Rev. A **69**, 022502 (2004).
[14] N. Bouloufa, A. Crubellier, and O. Dulieu, Phys. Rev. A **75**, 052501 (2007).
[15] D. Antypas and D. S. Elliott, Phys. Rev. A **88**, 052516 (2013).
[16] M. S. Safronova and C. W. Clark, Phys. Rev. A **69**, 040501(R) (2004).
[17] E. Iskrenova-Tchoukova, M. S. Safronova, and U. I. Safronova, J. Comp. Methods in Sciences and Engineering **7**, 521 (2007).
[18] S. G. Porsev, K. Beloy, and A. Derevianko, Phys. Rev. D **82**, 036008 (2010).
[19] A. Khadjavi, A. Lurio, and W. Happer, Phys. Rev. **167**, 128 (1968).
[20] G. Khvostenko and M. Chaika, Optica Spektrosk. **25**, 450 (1968) [Opt. and Spectrosc. **25**, 246 (1968)].
[21] V. G. Domelunksen, Optica Spektrosk. **54**, 950 (1983) [Opt. and Spectrosc. **54**, 565 (1983)].
[22] E. Arimondo, M. Inguscio, and P. Violino, Rev. Mod. Phys. **49**, 31 (1977).
[23] W. A. van Wijngaarden and J. Li, J. Quant. Spectrosc. Radiat. Transfer **52**, 555 (1994).
[24] R. W. Schmieder, Am. J. Phys. **40**, 297 (1972).
[25] C. E. Tanner and C. Wieman, Phys. Rev. A **38**, 162 (1988).
[26] W. A. van Wijngaarden, E. A. Hessels, J. Li, and N. E. Rothery, Phys. Rev. A **49**, R2220 (1994).
[27] D. Antypas and D. S. Elliott, Phys. Rev. A **83**, 062511 (2011).
[28] A. Kortyna, C. Tinsman, J. Grab, M. S. Safronova, and U. I. Safronova, Phys. Rev. A **83**, 042511 (2011).
[29] D. Antypas and D. S. Elliott, Phys. Rev. A **87**, 042505 (2013).
[30] D. Antypas and D. S. Elliott, Can. J. of Chem. **92**, 144 (2014).
[31] P. W. Pace and J. B. Atkinson, Can. J. Phys. **53**, 937 (1975).
[32] E. Campani, G. Degan, and G. Gorini, Lett. Nuovo Cimento **23**, 187 (1978).
[33] M. Ortiz and J. Campos, J. Quant. Spectrosc. Radiat. Transfer **26**, 107 (1981).
[34] H. Kleiman, J. Opt. Soc. Am. **52**, 441 (1962).
[35] K. B. Eriksson, I. Johansson, and G. Norlén, Ark. Fys. **28**, 233 (1965).